The Astrophysical Journal Letters, 963:L30 (6pp), 2024 March 1 https://doi.org/10.3847/2041-8213/ad28b7

Evidence of High-latitude Emission in the Prompt Phase of GRBs: How Far from the Central Engine are the GRBs Produced?

Z. Lucas Uhm[1], Donggeun Tak[1,2,3], Bing Zhang[4], Judith Racusin[5], Daniel Kocevski[6], Sylvain Guiriec[5,7], Bin-Bin Zhang[8], and Julie McEnery[5,9]
[1] Korea Astronomy and Space Science Institute, Daejeon 34055, Republic of Korea; uhm@kasi.re.kr
[2] SNU Astronomy Research Center, Seoul National University, Seoul 08826, Republic of Korea
[3] Deutsches Elektronen-Synchrotron DESY, Platanenallee 6, 15738 Zeuthen, Germany
[4] Department of Physics and Astronomy, University of Nevada, Las Vegas, NV 89154, USA
[5] Astrophysics Science Division, NASA Goddard Space Flight Center, Greenbelt, MD 20771, USA
[6] Astrophysics Office, ST12, NASA Marshall Space Flight Center, Huntsville, AL 35812, USA
[7] Department of Physics, The George Washington University, Washington, DC 20052, USA
[8] School of Astronomy and Space Science, Nanjing University, Nanjing 210093, People's Republic of China
[9] Department of Physics, University of Maryland, College Park, MD 20742, USA
Received 2022 December 14; revised 2024 January 19; accepted 2024 February 12; published 2024 February 29

Abstract

One of the difficulties in nailing down the physical mechanism of gamma-ray bursts (GRBs) comes from the fact that there has been no clear observational evidence on how far from the central engine the prompt gamma rays of GRBs are emitted. Here we present a simple study addressing this question by making use of the "high-latitude emission" (HLE). We show that our detailed numerical modeling exhibits a clear signature of HLE in the decaying phase of "broad pulses" of GRBs. We show that the HLE can emerge as a prominent spectral break in F_ν spectra and dominate the peak of νF_ν spectra even while the "line-of-sight emission" (LoSE) is still ongoing. This finding provides a new view of HLE emergence since it has been believed so far that the HLE can show up and dominate the spectra only after the LoSE is turned off. We remark, however, that this "HLE break" can be hidden in some broad pulses, depending on the proximity between the peak energies of the LoSE and the HLE. Therefore, this new picture of HLE emergence explains both the detection and nondetection of HLE signature in observations of broad pulses. Also, we present three examples of Fermi Gamma-ray Burst Monitor GRBs with broad pulses that exhibit the HLE signature. We show that their gamma-ray-emitting region should be located at $\sim 10^{16}$ cm from the central engine, which places a constraint on the GRB models.

Unified Astronomy Thesaurus concepts: Gamma-ray bursts (629); Non-thermal radiation sources (1119); Relativistic jets (1390)

1. Introduction

The gamma-ray bursts (GRBs) are believed to invoke highly relativistic jets with bulk Lorentz factors of a few hundred (Kumar & Zhang 2015). For such a highly relativistic jet, the relativistic beaming and boosting of radiation plays an important role and gives rise to interesting results especially when combined with a spherical geometry of the emitting surface. The photons emitted from a jet location with high latitude, called the "high-latitude emission" (HLE), take longer to reach a distant observer and are boosted with a smaller Doppler factor than the photons traveling along the line of sight, called the "line-of-sight emission" (LoSE). These two aspects of HLE are known as the "curvature effect" of a relativistic spherical jet. It is known that the HLE satisfies a simple relation (Kumar & Panaitescu 2000; Dermer 2004; Uhm & Zhang 2015), $\hat{\alpha} = 2 + \hat{\beta}$, between the temporal index $\hat{\alpha}$ and the spectral index $\hat{\beta}$ in the convention of $F_{\nu_{\rm obs}} \propto t_{\rm obs}^{-\hat{\alpha}}\, \nu_{\rm obs}^{-\hat{\beta}}$ if the emitter remains a constant Lorentz factor. Here, $F_{\nu_{\rm obs}}$ is the observed spectral energy flux, $t_{\rm obs}$ the observer time, and $\nu_{\rm obs}$ the observed frequency. This relation was generalized later for relativistic jets that undergo bulk acceleration ($\hat{\alpha} > 2 + \hat{\beta}$) or bulk deceleration ($\hat{\alpha} < 2 + \hat{\beta}$) (Uhm & Zhang 2015).

The curvature effect of HLE is commonly invoked to account for the steep decay of GRB flares observed in X-rays (e.g., Liang et al. 2006; Uhm & Zhang 2016a; Jia et al. 2016) and gamma rays (Ajello et al. 2019). This effect is also employed to explain the early steep decay during the transition from the prompt emission to the afterglow in the X-ray (e.g., Zhang et al. 2006, 2009; Hascoët et al. 2012) and GeV energy bands (Ajello et al. 2019). As for the prompt phase of GRBs, several studies (Ryde & Petrosian 2002; Kocevski et al. 2003; Genet & Granot 2009; Shenoy et al. 2013) have investigated the role that the curvature effect has on temporal and spectral properties of individual pulses, but an unambiguous identification of HLE could not be achieved.

The prompt phase of GRBs contains an important observational feature called the "broad pulses." Observationally, the broad pulses exhibit two distinct patterns of peak evolution; i.e., the peak energy (E_p) of νF_ν spectra shows a "hard-to-soft" or a "flux-tracking" pattern across the pulses (Golenetskii et al. 1983; Ford et al. 1995; Norris et al. 1996; Lu et al. 2012). In addition, the lightcurves of broad pulses in different energy bands exhibit a sequential pattern in their peak time, known as the "spectral lags" (Norris et al. 1996, 2000; Kocevski & Liang 2003); softer emission lags behind harder emission ("positive" type) in most cases, whereas harder emission can lag behind softer emission ("negative" type) in some cases. The

curvature effect of HLE was traditionally suggested as a plausible explanation for the positive type of spectral lags (Shen et al. 2005), but a detailed study (Uhm & Zhang 2016b) showed that the HLE cannot give rise to any spectral lags if the spectral shape is softer than $F_{\nu_{\rm obs}} \propto \nu_{\rm obs}^2$. The HLE may produce some spectral lags for a spectral shape harder than this $\nu_{\rm obs}^2$, but the resulting spectral lags are essentially invisible due to the significant flux-level difference between the lightcurves (Uhm & Zhang 2016b).

The complex and intriguing characteristics of broad pulses carry crucial clues to unveil the nature of GRBs. For instance, a series of numerical studies (Uhm & Zhang 2016b; Uhm et al. 2018) showed that all those features of broad pulses can be successfully reproduced within a single physical picture that invokes a bulk acceleration of the emitting region and that keeps the LoSE ongoing across the production of broad pulses. Also, Li & Zhang (2021) found evidence of jet acceleration in an effort to search for the curvature effect.

Here, we present a simple study that identifies a clear signature of HLE in the decaying phase of broad pulses and provide a new understanding of the HLE emergence. We also present three examples of Fermi Gamma-ray Burst Monitor (GBM; Meegan et al. 2009) GRBs that exhibit the HLE signature in their broad pulses.

2. A Simple Physical Model

Following the previous works (Uhm & Zhang 2016b; Uhm et al. 2018), we adopt a simple physical picture where a thin, relativistic spherical shell expands in space radially. The radiating electrons are distributed uniformly in the shell and emit synchrotron photons (Rybicki & Lightman 1979) isotropically in the comoving frame. Then, we take fully into account the curvature effect to compute the HLE (Uhm & Zhang 2015). We assume a "Band" function shape (Band et al. 1993) for the emission spectrum in the comoving frame since the observed gamma-ray spectra are traditionally fit to this function and since it is a good representation of synchrotron radiation (Uhm & Zhang 2014; Zhang et al. 2016). The strength of magnetic field $B(r)$ in the emitting region globally decreases as the radius r from the central engine increases, which is expected for a spherical jet traveling in space. We note that this was the essential physical element to explain the low-energy photon index of the Band spectra for the majority of GRBs (Uhm & Zhang 2014; Geng et al. 2018). Moreover, the emitting region itself undergoes rapid bulk acceleration (Uhm & Zhang 2016a, 2016b) during which the prompt gamma rays are produced, i.e., the bulk Lorentz factor $\Gamma(r)$ of the region has an increasing profile in radius r. Also, the characteristic Lorentz factor $\gamma_{\rm ch}(r)$ of electrons in the comoving frame is allowed to evolve with radius r.

We present three numerical models of broad pulses: Models [u], [v], and [w]. The three models have different $\gamma_{\rm ch}(r)$ profiles as described in the Appendix. Other than the $\gamma_{\rm ch}$ profile, we keep all other model parameters the same for the three models, for simplicity. We assume a Band-function shape with typical low- and high-energy photon spectral indexes $\alpha_{\rm B} = -0.8$ and $\beta_{\rm B} = -2.3$, respectively, for the emission spectrum in the comoving frame. The number of radiating electrons is assumed to increase at a constant injection rate $R_{\rm inj} = 10^{47}\ {\rm s}^{-1}$. The bulk Lorentz factor of the jet takes a power-law profile in radius r, $\Gamma(r) = \Gamma_0 (r/r_0)^s$, with $\Gamma_0 = 250$, $r_0 = 10^{15}$ cm, and $s = 0.35$, as used in Uhm & Zhang (2016b). We turn on the emission of the spherical jet at radius $r_{\rm on} = 10^{14}$ cm and turn off its emission at radius $r_{\rm off} = 3 \times 10^{16}$ cm. For the given profile of $\Gamma(r)$, this turning-off happens at about $t_{\rm obs} = 4.0$ s. We stress that the LoSE remains ongoing until this turn-off time. The magnetic field strength $B(r)$ in the comoving frame also takes a power-law profile, $B(r) = B_0 (r/r_0)^{-b}$, with $B_0 = 30$ G and $b = 1.5$ (Uhm & Zhang 2016b). We calculate the luminosity distance to GRB for a flat ΛCDM Universe with parameters $\Omega_{\rm m} = 0.31$, $\Omega_\Lambda = 0.69$, and $H_0 = 68$ km s^{-1} Mpc^{-1} (Planck Collaboration et al. 2016) and take a typical value of redshift $z = 1$.

3. Results of Numerical Models

Figure 1 shows a modeling result of the three models [u], [v], and [w]. The top panels show the lightcurves at 100 keV, 300 keV, and 1 MeV, which exhibit both the positive and negative types of spectral lags. The top panels also show the temporal evolution of E_p curves exhibiting both the hard-to-soft and the flux-tracking patterns across the pulses. We plot the E_p points up to $t_{\rm obs} = 4.0$ s during which the LoSE remains ongoing. Note that the breaks in E_p curves are due to the breaks in $\gamma_{\rm ch}$ profiles (see the Appendix). The lightcurves at 1 MeV also show features linked with the $\gamma_{\rm ch}$ evolution. The middle panels show the time-dependent spectra at 1, 2, and 3 s (solid lines). In the comoving frame, we inject a Band-function spectrum with fixed $\alpha_{\rm B}$ and $\beta_{\rm B}$. However, the resulting spectra in the observer frame deviate significantly from this single Band function. Hence, in order to understand this deviation, we repeat the same calculations without considering the curvature effect, and the resulting spectra are shown in dotted lines in the middle panel for model [u]. Comparing the solid and dotted lines, one can clearly see that the curvature effect causes the deviation and that the HLE emerges as a prominent additional spectral break in F_ν spectra during the decaying phase of the broad pulses.[10] We stress again that the jet emission is not turned off until about 4 s in our models and, therefore, the LoSE is still active and dominates the peak of F_ν spectra as it should. The bottom panels show the νF_ν spectra directly calculated from the solid lines in the middle panels, in which it is clear that the "HLE break" ($\nu_{\rm HLE}$) in F_ν spectra now becomes the peak energy (E_p) in νF_ν spectra in the decaying phase of these broad pulses.

We add a remark that an introduction of a break in the profile of $\Gamma(r)$ and/or $B(r)$ induces only a marginal difference and keeps our results unchanged.

If the peak of νF_ν spectra is dominated by the HLE in the falling phase of broad pulses, there should exist a simple scaling relation,

$$F_{\nu,E_p} \propto E_p^{\,2}, \tag{1}$$

expected from the HLE theory (Dermer 2004; Uhm & Zhang 2015). Here, F_{ν,E_p} is the spectral energy flux F_ν measured at the peak energy E_p.

In Figure 2, we plot F_{ν,E_p} against E_p across the broad pulses of three numerical models [u], [v], and [w]. An open circle in each model marks the first point at the beginning of the pulse. One can clearly see that the model curves closely follow Equation (1) (indicated by the dotted line) in the decaying phase of broad pulses, ascertaining that the peak of νF_ν spectra

[10] We remark that the HLE emergence is modest in model [w] due to a second activity occurring right before 2 s.

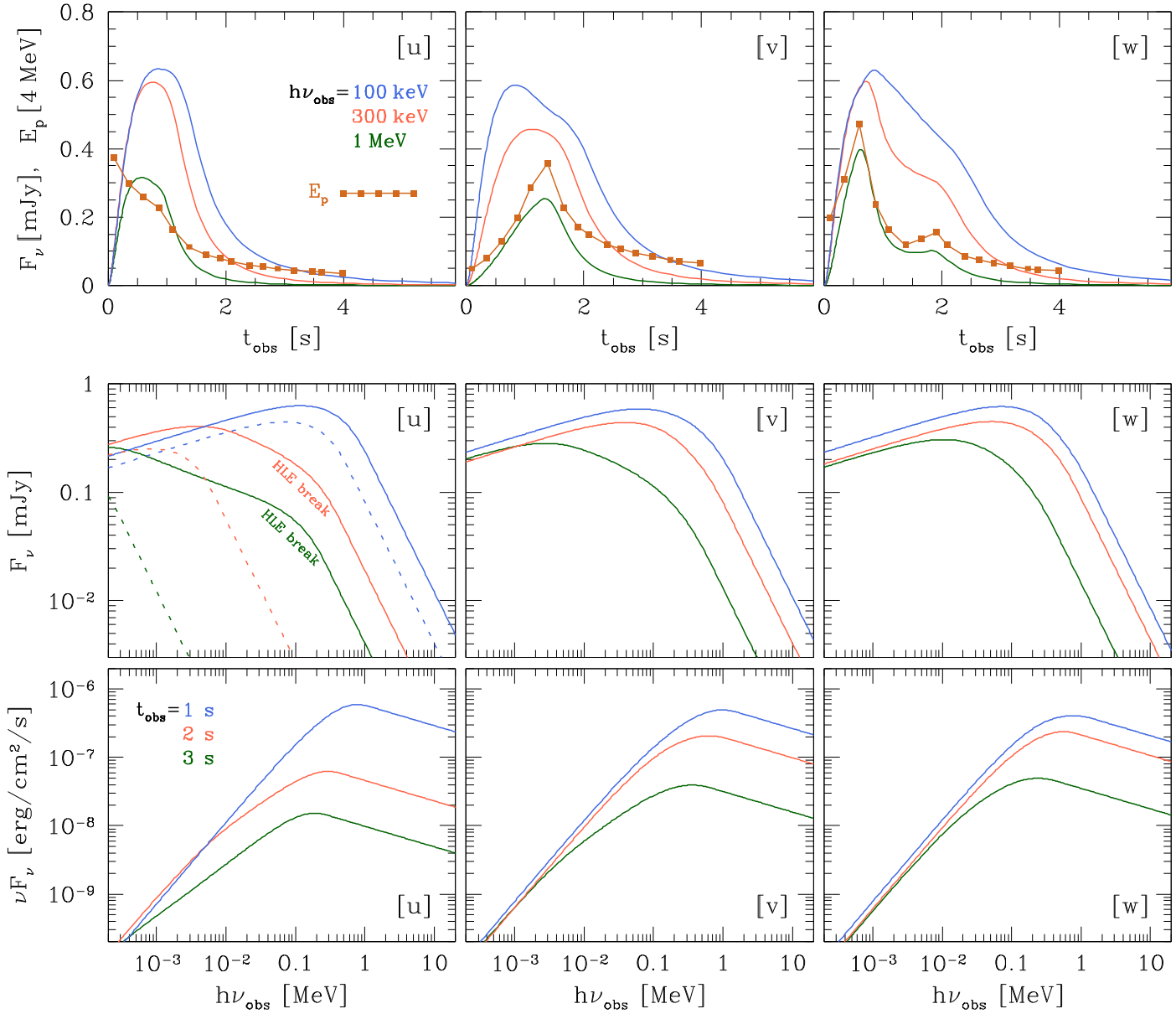

Figure 1. Lightcurves and time-dependent spectra of our numerical models [u], [v], and [w]. The top panels show the lightcurves at 100 keV, 300 keV, and 1 MeV, together with the temporal evolution of E_p curves. The middle panels show time-dependent spectra at 1, 2, and 3 s, with the curvature effect of HLE (Uhm & Zhang 2015) fully included (solid lines) or removed (dotted lines) for model [u]. The νF_ν spectra in the bottom panels are derived from the corresponding solid lines in the middle panels.

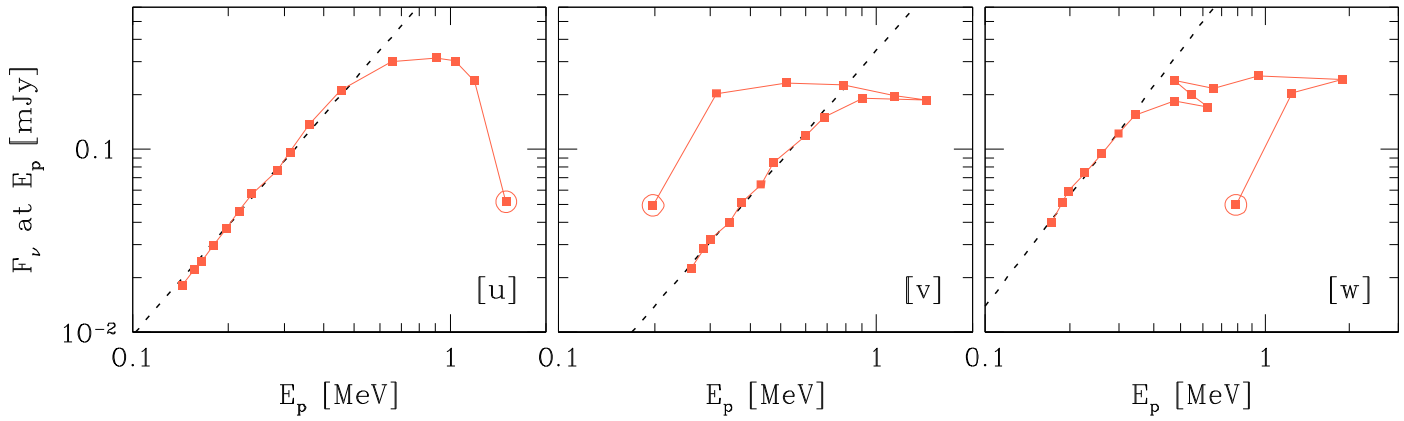

Figure 2. The peak energy E_p vs. the spectral flux F_ν at E_p (i.e., F_{ν,E_p}) across the broad pulses of our numerical models [u], [v], and [w]. An open circle in each model marks the first point at the beginning of pulses. The dotted line indicates the relation $F_{\nu,E_p} \propto E_p^2$ in Equation (1).

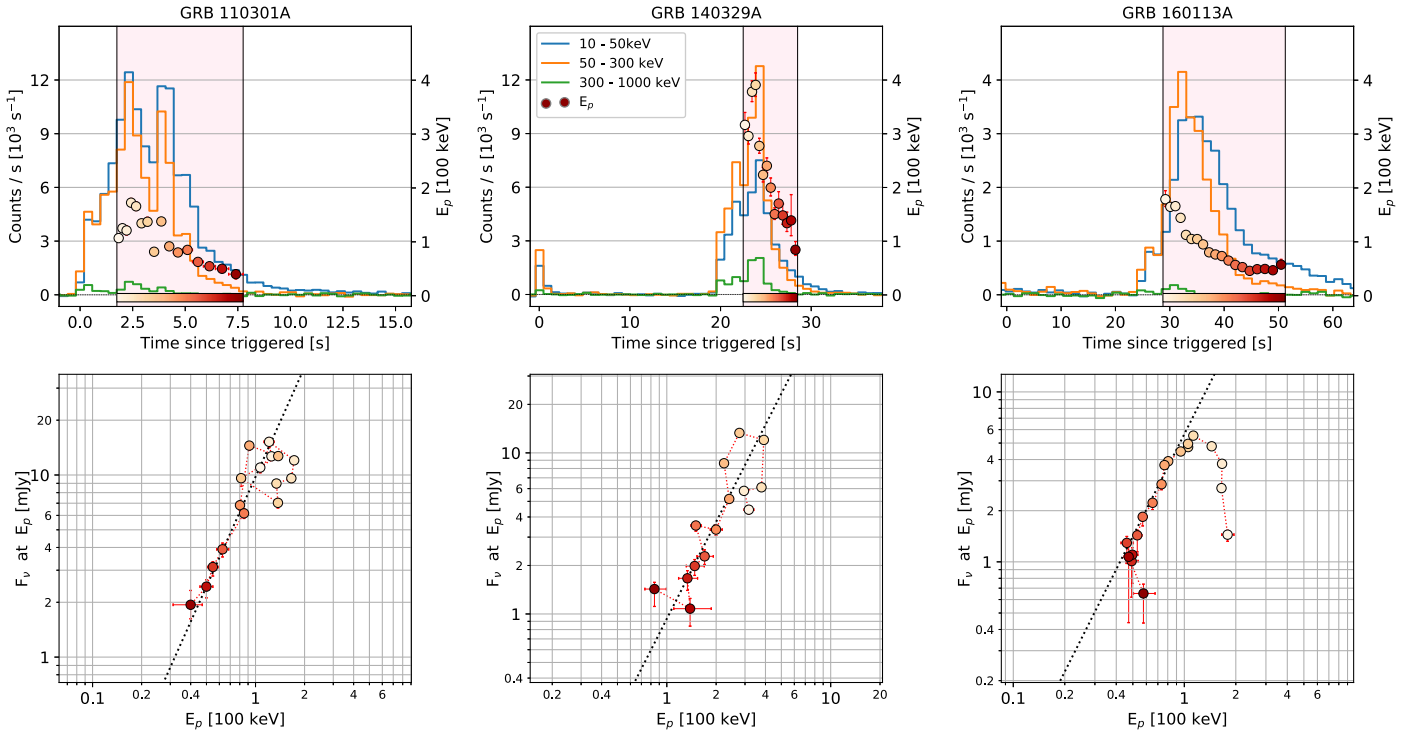

Figure 3. Results of our time-resolved spectral analysis performed on three example broad pulses in GRB 110301A, GRB 140329A, and GRB 160113A. The top panels show the lightcurves at three different energy bands, together with the temporal evolution of E_p points. The bottom panels show the E_p vs. F_{ν,E_p} points obtained from the analysis. The dotted line indicates the relation $F_{\nu,E_p} \propto E_p^2$ in Equation (1). The color gradient in the bottom panels is in accordance with the color gradient encoded in the E_p points in the top panels.

indeed originates from the HLE. This is the clear signature of HLE, produced in our numerical models of broad pulses.

4. Search for the HLE Signature in Observations

Fermi-GBM (Meegan et al. 2009) has accumulated invaluable observations for the prompt emission of GRBs. In search of the HLE signature above, we analyze a sample of Fermi-GBM GRBs with relatively clean broad pulses and perform a dedicated time-resolved spectral analysis[11] for each broad pulse; see our companion paper Tak et al. (2023) for details.

In Figure 3, we present three examples: GRB 110301A, GRB 140329A, and GRB 160113A. The top panels show the lightcurves at three different energy bands, together with the temporal evolution of E_p curves. The bottom panels show E_p versus F_{ν,E_p} obtained from the time-resolved spectral analysis. The dotted line indicates the theoretical HLE relation in Equation (1). As one can see, the E_p vs. F_{ν,E_p} points obtained from the time-resolved analysis of the three bursts are in good agreement with Equation (1) in the decaying phase of their broad pulse, implying that the HLE signature is indeed identified. The color gradient used in the bottom panels is in accordance with the color gradient encoded in the E_p points in the top panels, which helps locate where in the pulse the HLE signature starts to show up.

While numerous studies have explored the correlation between E_p and flux, this HLE signature we investigate has not been reported. This is primarily because most empirical relations are derived during the brightest phase of GRBs, whereas our study focuses on the falling phase of the broad pulses. Further details on the outcomes can be found in Tak et al. (2023).

[11] We test three widely used spectral models with freely varying parameters: the power-law (PL) function, the PL with an exponential cutoff, and the Band function. We determine the best-fit model and its parameters using a proper statistical method.

5. Conclusions and Discussion

In this Letter, we showed that the HLE can imprint a clear spectral signature in prompt-emission gamma-ray spectra (as an additional spectral break $\nu_{\rm HLE}$ in F_ν spectra and as the peak energy in νF_ν spectra) even with the existence of ongoing LoSE. This result provides a new view regarding the HLE because it has been believed so far that the HLE can show up and dominate the spectra only after the LoSE is turned off.

We remark, however, that the HLE spectral break is not required to appear in all broad pulses. It is because the HLE break can be buried under the ongoing LoSE component when the peak energy of LoSE (at a given time) is not far below that of HLE (emitted at earlier times but belonging to the same equal-arrival-time surface). Therefore, this new perspective on the HLE emergence provides flexibility to explain both the detection and the nondetection of an HLE signature in observations of broad pulses.

The location of the LoSE peak depends on the physical parameters in the emitting region, and in our models, it is roughly given by

$$\nu_{\rm LoSE} \propto \Gamma B \gamma_{\rm ch}^2 \propto r^{s-b+2g} \propto t_{\rm obs}^{(s-b+2g)/(1-2s)}, \quad (2)$$

where we assumed $\gamma_{\rm ch}(r) \propto r^g$ and used the relation $t_{\rm obs} \propto r/\Gamma^2 \propto r^{1-2s}$. On the other hand, the HLE break is expected to evolve in time as

$$\nu_{\rm HLE} \propto t_{\rm obs}^{-1}, \quad (3)$$

obeying the property of HLE. Therefore, we have the ratio of the two frequencies as

$$\frac{\nu_{\rm LoSE}}{\nu_{\rm HLE}} \propto t_{\rm obs}^{-(s+b-2g-1)/(1-2s)}. \quad (4)$$

When $\nu_{\rm LOSE}$ is sufficiently smaller than $\nu_{\rm HLE}$ (i.e., $\nu_{\rm LOSE}/\nu_{\rm HLE} \ll 1$), one can expect that the HLE break shows up in F_ν spectra and the HLE dominates the peak of νF_ν spectra.

The falling phase of the lightcurves in our numerical models shows a steep decay and satisfies the well-known closure relation, $\hat{\alpha} = 2 + \hat{\beta}$; specifically, $\hat{\alpha} \sim 3.3$ and $\hat{\beta} \sim 1.3$. This suggests that, even when the LoSE remains ongoing, the early steep decay phase following the prompt emission can be interpreted as the HLE of the prompt emission tail.

In this Letter, we also presented three Fermi-GBM broad pulses that exhibit the HLE scaling relation between E_p and F_{ν,E_p} (Equation (1)) in their decaying phase.

The HLE signature observed in some broad pulses leads to important implications regarding the emission radius of GRBs. The HLE emitted at radius r is received at an observer time given roughly by $t_{\rm obs} \sim r/(2c\,\Gamma^2)$ like in the case of LoSE, which yields

$$r \sim 2c\,\Gamma^2\,t_{\rm obs} = (1.6 \times 10^{16}\ {\rm cm})\left(\frac{\Gamma}{300}\right)^2\left(\frac{t_{\rm obs}}{3\ {\rm s}}\right), \quad (5)$$

where c is the speed of light. The duration of broad pulses in our examples is tens of seconds, and therefore the gamma-ray-emitting region of those GRBs with HLE signature should be located at $\sim 10^{16}$ cm from the central engine for a typical value of $\Gamma = 300$ (Ghirlanda et al. 2018). For a broad range of Γ spanning from 100 to 1000 (e.g., Piran 1999), the emission radius varies from $\sim 10^{15}$ to $\sim 10^{17}$ cm.

This inference of the emission radius is independent of the details of our modeling and sheds light on constraining the GRB models. The estimated large emission radius is consistent with the ICMART model (Zhang & Yan 2011), which invokes collision-induced magnetic dissipation as the origin of GRB prompt emission. In addition, this implies that some GRB models, such as classical photospheric emission models and small-radii internal shock models, face challenges[12] and demand modifications to account for those GRBs exhibiting the HLE signature.

In short, we identified a clear signature of HLE in the prompt phase of GRBs both theoretically and observationally. Also, we presented a unique constraint on the validity of the competing GRB models.

Acknowledgments

This work was supported by the National Research Foundation of Korea (NRF) grant No. 2021M3F7A1084525, funded by the Korea government (MSIT). B.B.Z. acknowledges the support by the National Key Research and Development Programs of China (2018YFA0404204, 2022YFF0711404, and 2022SKA0130102), the National Natural Science Foundation of China (grant Nos. 11833003, U2038105, and 12121003), the science research grants from the China Manned Space Project with No. CMS-CSST-2021-B11, and the Program for Innovative Talents, Entrepreneur in Jiangsu.

[12] The HLE exists in these models as well but the related timescales are much shorter than the duration of broad pulses by orders of magnitude. Therefore, the scaling relation in Equation (1) cannot be observed in the decaying phase of broad pulses unless their central engine behaves in a specific manner to produce this scaling relation, which is too contrived.

Appendix
Profile of Characteristic Lorentz Factor $\gamma_{\rm ch}$ of Electrons

The characteristic Lorentz factor $\gamma_{\rm ch}$ of electrons evolves in radius r in our models. We expect that the rate of dissipation of internal energy will determine the values of $\gamma_{\rm ch}$. If we think of an episode of energy dissipation, the dissipation may initially occur in an explosive manner such that $\gamma_{\rm ch}$ increases initially, which could be followed by a fading phase of dissipation with $\gamma_{\rm ch}$ decreasing. In this picture, it is plausible to assume that the $\gamma_{\rm ch}$ profile evolves in radius r as the emitting shell expands in space. The model [u] has a broken power-law profile:

$$\gamma_{\rm ch}(r) = \begin{cases} \gamma^0_{\rm ch}(r/r_0)^{g_1} & \text{if} \quad r < r_0, \\ \gamma^0_{\rm ch}(r/r_0)^{g_2} & \text{if} \quad r \geqslant r_0, \end{cases} \quad (A1)$$

with $\gamma^0_{\rm ch} = 10^5$, $r_0 = 10^{15}$ cm, $g_1 = 1/2$, and $g_2 = -1$. The model [v] also takes the same form of broken power-law but with $\gamma^0_{\rm ch} = 2 \times 10^5$, $r_0 = 2 \times 10^{15}$ cm, $g_1 = 1$, and $g_2 = -1$. The model [w] has a profile made of four power-law segments:

$$\gamma_{\rm ch}(r) = \begin{cases} \gamma^0_{\rm ch}(r/r_1) & \text{if} \quad r < r_1, \\ \gamma^0_{\rm ch}(r/r_1)^{-1} & \text{if} \quad r_1 \leqslant r < r_2, \\ 2\gamma^0_{\rm ch}(r/r_3) & \text{if} \quad r_2 \leqslant r < r_3, \\ 2\gamma^0_{\rm ch}(r/r_3)^{-1} & \text{if} \quad r_3 \leqslant r, \end{cases} \quad (A2)$$

with $\gamma^0_{\rm ch} = 10^5$, $r_1 = 5 \times 10^{14}$ cm, $r_2 = 10^{15}$ cm, and $r_3 = 4 \times 10^{15}$ cm. These three $\gamma_{\rm ch}$ profiles are shown in Figure 4.

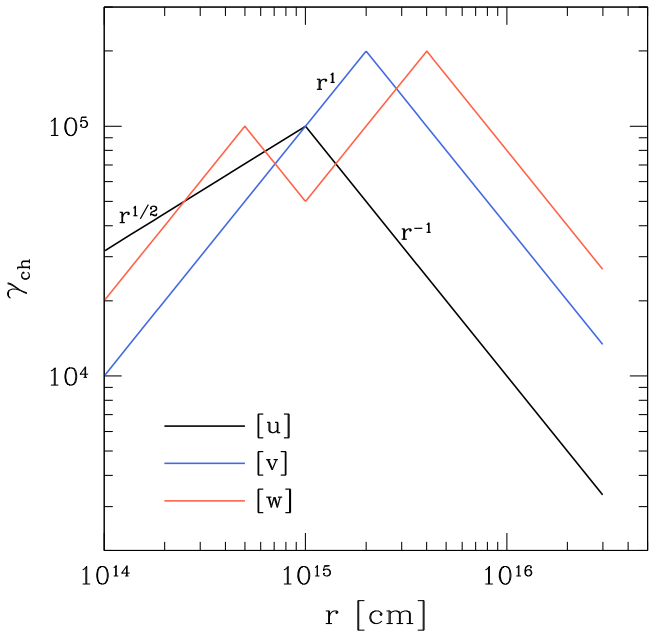

Figure 4. Profile of characteristic Lorentz factor $\gamma_{\rm ch}$ of electrons in our numerical models [u], [v], and [w].

ORCID iDs

Donggeun Tak https://orcid.org/0000-0002-9852-2469
Bing Zhang https://orcid.org/0000-0002-9725-2524
Judith Racusin https://orcid.org/0000-0002-4744-9898
Daniel Kocevski https://orcid.org/0000-0001-9201-4706
Sylvain Guiriec https://orcid.org/0000-0001-5780-8770
Bin-Bin Zhang https://orcid.org/0000-0003-4111-5958

References

Ajello, M., Arimoto, M., Asano, K., et al. 2019, ApJL, 886, L33
Band, D., Matteson, J., Ford, L., et al. 1993, ApJ, 413, 281
Dermer, C. D. 2004, ApJ, 614, 284
Ford, L. A., Band, D. L., Matteson, J. L., et al. 1995, ApJ, 439, 307
Genet, F., & Granot, J. 2009, MNRAS, 399, 1328
Geng, J.-J., Huang, Y.-F., Wu, X.-F., Zhang, B., & Zong, H.-S. 2018, ApJS, 234, 3
Ghirlanda, G., Nappo, F., Ghisellini, G., et al. 2018, A&A, 609, A112
Golenetskii, S. V., Mazets, E. P., Aptekar, R. L., & Ilinskii, V. N. 1983, Natur, 306, 451
Hascoët, R., Daigne, F., & Mochkovitch, R. 2012, A&A, 542, L29
Jia, L.-W., Uhm, Z. L., & Zhang, B. 2016, ApJS, 225, 17
Kocevski, D., & Liang, E. 2003, ApJ, 594, 385
Kocevski, D., Ryde, F., & Liang, E. 2003, ApJ, 596, 389
Kumar, P., & Panaitescu, A. 2000, ApJL, 541, L51
Kumar, P., & Zhang, B. 2015, PhR, 561, 1
Li, L., & Zhang, B. 2021, ApJS, 253, 43
Liang, E. W., Zhang, B., O'Brien, P. T., et al. 2006, ApJ, 646, 351
Lu, R.-J., Wei, J.-J., Liang, E.-W., et al. 2012, ApJ, 756, 112
Meegan, C., Lichti, G., Bhat, P. N., et al. 2009, ApJ, 702, 791
Norris, J. P., Marani, G. F., & Bonnell, J. T. 2000, ApJ, 534, 248
Norris, J. P., Nemiroff, R. J., Bonnell, J. T., et al. 1996, ApJ, 459, 393
Piran, T. 1999, PhR, 314, 575
Planck Collaboration, Ade, P. A. R., Aghanim, N., et al. 2016, A&A, 594, A13
Rybicki, G. B., & Lightman, A. P. 1979, Radiative processes in astrophysics, 1979 (New York: Wiley-Interscience), 393
Ryde, F., & Petrosian, V. 2002, ApJ, 578, 290
Shen, R.-F., Song, L.-M., & Li, Z. 2005, MNRAS, 362, 59
Shenoy, A., Sonbas, E., Dermer, C., et al. 2013, ApJ, 778, 3
Tak, D., Uhm, Z. L., Racusin, J., et al. 2023, ApJ, 949, 110
Uhm, Z. L., & Zhang, B. 2014, NatPh, 10, 351
Uhm, Z. L., & Zhang, B. 2015, ApJ, 808, 33
Uhm, Z. L., & Zhang, B. 2016a, ApJL, 824, L16
Uhm, Z. L., & Zhang, B. 2016b, ApJ, 825, 97
Uhm, Z. L., Zhang, B., & Racusin, J. 2018, ApJ, 869, 100
Zhang, B., Fan, Y. Z., Dyks, J., et al. 2006, ApJ, 642, 354
Zhang, B., & Yan, H. 2011, ApJ, 726, 90
Zhang, B.-B., Uhm, Z. L., Connaughton, V., Briggs, M. S., & Zhang, B. 2016, ApJ, 816, 72
Zhang, B.-B., Zhang, B., Liang, E.-W., & Wang, X.-Y. 2009, ApJL, 690, L10